# Coded 64-CAP ADSL in an Impulse-Noise Environment—Modeling of Impulse Noise and First Simulation Results

Werner Henkel, *Member, IEEE,* Thomas Kessler, and Hong Y. Chung, *Member, IEEE*

*Abstract*—**This paper presents the performance of various coding schemes for the asymmetrical digital subscriber line (ADSL) in an impulse-noise environment. Impulse noise is considered to be one of the most damaging impairments in the ADSL, in which compressed video signals are delivered to residential customers. The impulse noise used in this study was measured and collected in German telephone networks. Based on this measurement and the corresponding statistical modeling, a simulation model for impulse noise is proposed and its properties are outlined.**

**The coding schemes considered here utilize burst-error correcting Reed–Solomon codes and/or random error correcting trellis codes as well as symbol interleaving between the two codes. It has been found through computer simulations that a proper concatenation of the two codes could increase the immunity against impulse noise compared to an uncoded scheme. Specifically, a concatenated code, using a 2-dimensional 8-state trellis code and a 4-error-correcting Reed–Solomon code with an interleaving depth of 18 symbols, was able to eliminate all the errors caused by the impulse noise used in the study. It has also been found that the trellis codes are not very effective against impulse noise, unless they are used in conjunction with Reed–Solomon codes and a proper symbol interleaving. Performance results of other coding configurations using Reed–Solomon codes with different error-correcting capabilities are also presented. In addition, we also show the performance results when simple array codes are used instead of the Reed–Solomon codes.**

## I. Introduction

THE asymmetrical digital subscriber line (ADSL) [1], [2] provides very high bit-rate video services to residential customers over unshielded twisted pairs. The ADSL operates at a data rate of 1.544 Mb/s for primary T1 rate and 2.048 Mb/s for E1 rate over subscriber loops from the central office (CO) to the customer, and a lower rate control channel is provided for the other direction. Since the copper medium used for ADSL services suffers a high propagation loss and a possible cross-talk (NEXT) from other types of services as the transmission length and the signal bandwidth increase, the ADSL requires a bandwidth-efficient modulation scheme that can reliably carry the information. Carrierless amplitude/phase (CAP) modulation [3], which is a variant of quadrature amplitude modulation (QAM), is well suited for this type of application, because of its inherent bandwidth-efficiency and the compatibility with error-correcting codes. The ADSL, however, also suffers from impulse noise. Impulse noise caused by relay reopenings and from various other sources [4] can have a significant impact on compressed video signals in the ADSL. Although it is well known that the trellis-coded modulation (TCM) [5] used in conjunction with CAP or QAM can provide 3–5 dB coding gains in an additive white Gaussian noise (AWGN) environment where random errors are dominant, it may not be able to provide the same performance in an environment where bursty or colored noise such as NEXT are dominant. Bursty errors are usually generated by an impulse noise and can also result from NEXT affecting consecutive symbols in the Viterbi decoder, because such a decoder relies on the past history of the symbol sequence. Thus, a coding scheme is required for the ADSL that is robust against impulse noise in order to minimize its impact on the compressed video signals. Impulses that are used in this study were taken from one site of the German survey where the impulse noise was considered to have quite typical statistical properties. These will be described later in the paper.

It is the main purpose of this paper to present performance results of coding schemes using several component codes such as Reed–Solomon (RS) codes, array codes, and trellis codes to mitigate the effects of impulse noise. RS codes are well suited for ADSL application, because they are known to be very effective for correcting multiple bursts of errors [6]. Although array codes are not originally designed for correcting a burst of errors, we also investigate array codes with diagonal readout whose symbols are comprised of multiple bits [7]. These codes turned out to be able to provide a good error-correcting capability with a low decoding complexity at the receiving end as compared to RS codes.

The remainder of the paper is organized as follows. Section II gives an overview of the considered coding schemes that were applied to 64-CAP. In Section III, we briefly explain the method that was used to collect the impulses in German networks together with the results of the statistical modeling and possible simulation methods. Section IV provides error-performance results in impulse noise for the various configurations of coding schemes obtained by computer simulation. First a constant inter-arrival time is assumed, whereas Section V presents first results when using stochastic inter-arrival times supplied by a dedicated generator that follows the statistics described in Section III. Finally, discussions and a summary are given in Section VI.

Manuscript received June 20, 1994; revised May 10, 1995. This paper has been submitted in part to Globecom 95 and CTMC ([23]–[25]).

W. Henkel and T. Kessler are with the Research Center of Deutsche Telekom, D-64276 Darmstadt, Germany.

H. Y. Chung is with AT&T Bell Laboratories, Holmdel, NJ 07733 USA.

IEEE Log Number 9415310.

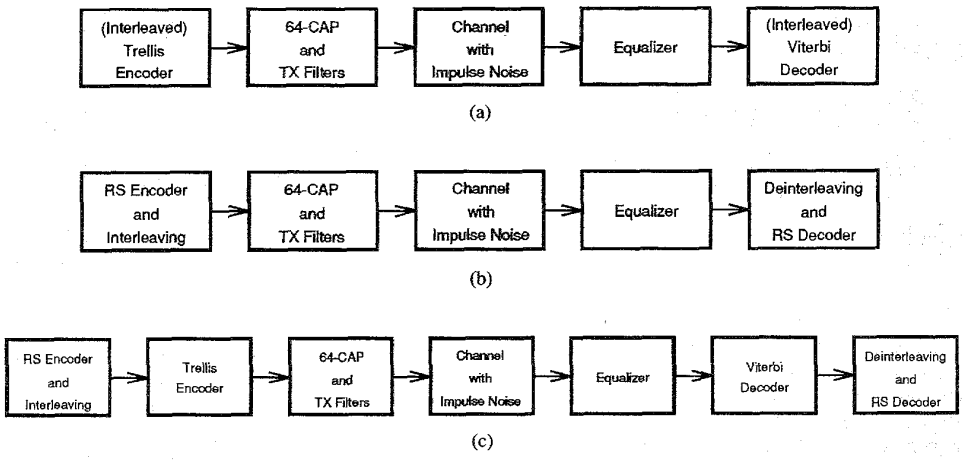


Fig. 1. Simulated coding schemes.

## II. System Description and Simulated Schemes

There are several coding schemes we consider for an impulse-dominated environment. These are either RS coded, trellis coded or both RS and trellis-coded CAP schemes. Array codes will also be used. The uncoded scheme that transmits the same data rate as the coded schemes will be used as a reference scheme throughout the paper. Some coded schemes will have interleaving to further distribute the errors after the decoder. However, it should be noted that the interleaving increases the overall transmission delay and should be designed to meet the delay specifications set by the customers.

In this section, we present block diagrams for the coded schemes that are simulated in this study. We start with a scheme that uses trellis code only, which is shown in Fig. 1(a). The trellis code used here is a 2-dimensional 8-state trellis code [8] and for the configuration shown in Fig. 1(a), the encoder encodes 5 information bits into 6 bits which in turn are mapped on to 64-CAP ($8 \times 8$) rectangular constellation.[1]

As mentioned before, the TCM in general is very effective in AWGN, providing significantly larger noise margin over an uncoded counterpart. However, in an impulse environment, because of the nature of the maximum-likelihood sequence estimation algorithm used in the decoding of trellis-coded symbols, it is not very effective when several consecutive received symbols are corrupted by impulse noise. We also simulated an interleaved trellis code, which utilizes more than one encoder and decoder in a time-multiplexed fashion. The effect of using this type of scheme is to distribute the errors caused by an impulse so that they could be corrected by trellis decoders. This, however, will increase the decoding delay by a factor of $n$, where $n$ is the number of encoder/decoder pairs used in parallel. Fig. 1(b) shows an RS coded scheme. The RS codes used here are for $t = 2$ (135, 131), $t = 3$ (135, 129), and $t = 4$, (135, 127), where $t$ denotes the symbol error-correcting capability of the code. In $(n, k)$ RS-coded cases, the signal bandwidth is increased by a factor of $n/k$. A concatenated code that uses both the RS code and the trellis code is shown in Fig. 1(c). The main idea of concatenating two or more codes together is to use the additional decoders to further correct the errors after the first decoder, if the output from the first decoder forms a correctable pattern for the additional decoders. Due to the constraints on delay and complexity, concatenated codes usually use only two codes, namely, inner and outer codes. The scheme can also use a symbol interleaving between the inner and outer codes to further distribute the errors at the output of the trellis decoder at the receiver. This might help the outer decoder to correct errors more efficiently. However, the interleaving depth, which defines the degree of interleaving should be chosen carefully not to affect the performance of the outer decoder. It will be shown later that a larger interleaving depth does not necessarily provide a better performance and can have an adverse effect on the outer decoder. Array codes are also used by replacing the RS codes shown in the figures. A more detailed information regarding the use of array codes will be given later in the paper.

[1] Although 64-CAP is used for all coded and uncoded schemes presented in this paper, other constellations can be used instead. Changing the number of signal points in the constellation, however, will change the signal bandwidth and, consequently, will slightly affect the overall performance.

## III. Impulse Noise

### A. Measurement Campaign of German Telekom

All the results described herein rely on an extensive measurement campaign, carried out at seven locations inside Germany (mainly at inter-office trunks) including one in the former GDR (eastern part of Berlin). Unlike earlier surveys [9]–[15], it consisted of wideband measurements with high timing resolution. At each location, impulses were recorded at a sampling rate of 10.24 MHz, voltage histograms were computed and inter-arrival times were stored. The equipment consisted of a processing storage oscilloscope together with a combined anti-aliasing filter (cut-off frequency 4.25 MHz), amplifier, and trigger unit.

One recorded impulse event has 4096 samples (400 $\mu$s), where 200 of them are pre-trigger samples. Altogether, 51 200 such impulse events were recorded per site. A few selected impulses are shown in Fig. 2.

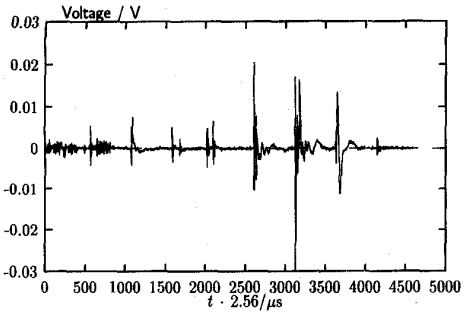


Fig. 2. Some sample impulses (location: Mayence).

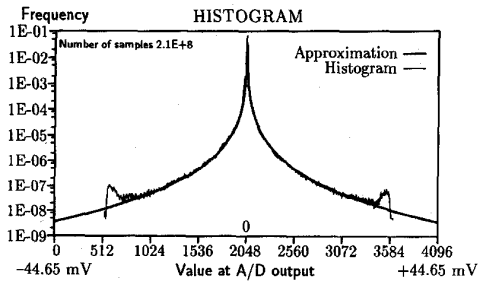


Fig. 3. Approximation of an impulse-noise voltage density in the case of low background noise (location: Mayence).

Two types of voltage histograms were processed. The first was computed directly at the measurement site, evaluating every 100th sample (to avoid a too strong influence of one single impulse). This measurement was freely running without any trigger condition. The total number of processed samples per location was $10^{10}$ at most. The second type of histograms was computed off-line from recorded impulses, evaluating every sample (not every 100th).

Furthermore, peak-voltage histograms were processed at three locations. They have not been used for our modeling purposes and are therefore not shown herein.

The inter-arrival time measurement had a resolution of 32 bits, ranging from 100 ns up to 7.2 min. At most $16 \cdot 10^6$ time samples were recorded at the different locations.

All the three measurements (recording of impulses, voltage histogram, and recording of inter-arrival times) were carried out independently one after another due to the measurement equipment.

For a comprehensive description of the measurements and their results, see [16]. Even more detailed information is available in the form of an internal report (in German) that can be obtained from the authors. A first short publication was also made in [17].

Besides our own campaign, two other surveys by British Telecom [18] and Bellcore [19] were recently carried out. The first resulted in some sort of representative test impulse with principal disadvantages. One impulse can, of course, not represent the statistics of real impulse noise. Furthermore, the defined impulse has a pole at time zero and infinite energy. The other survey was similar to ours, but could not lead to a statistical model, because of a too small number of samples and some shortcomings in the analysis. The following section gives a sketch of our statistical model of impulse noise.

### *B. Statistical Modeling of Voltage, Inter-Arrival Time, and Length Densities*

Herein, we shall describe modeling probability density functions (PDF's) for the voltage, the length and inter-arrival time statistics. Together with the spectral properties, this will lead to a generator model of impulse noise which will be discussed in Section III-D-2. However, the described generator combination has not yet been used for many cases of the CAP simulation, because when they were carried out, the complete generator configuration was not already tested. Therefore, the stored impulses were used directly. In Section V, the impulse insertion was activated by the inter-arrival time generator which is one component of the complete generator model.

*1) Probability Density Function of the Voltages:* The pure impulse-noise density function was modeled by

$$f_i(u) = \frac{1}{240u_0} e^{-|u/u_0|^{1/5}}, \qquad (u_0 > 0). \tag{1}$$

An approximation using this function for a frequency distribution at a location where nearly no additional background noise was superimposed, is shown in Fig. 3. This frequency distribution was derived from recorded impulses, although in this case, the on-line version looks very similar. The local maxima at the edges of the operating range are due to the way the histogram was determined. Note that for the histogram from recorded impulses every sample was evaluated, enabling single impulses to have a dominant effect on low-frequency portions of the histogram.

When background noise, recognized to be nearly Gaussian, is added, during an impulse event, the resulting density can approximately be described by the convolution of the Gaussian and impulse densities. Outside the impulse events, only Gaussian background noise is present. The following sum represents the total density.

$$f_{\text{tot}}(x) = N \cdot f_n(x) + (1 - N) \cdot f_i(x) \star f_n(x), \tag{2}$$

where

$$f_n(x) = \frac{1}{\sigma\sqrt{2\pi}} e^{-x^2/2\sigma^2}$$

is the Gaussian-noise density with $N \in [0, 1]$ being the percentage of impulse-free times.

*2) Probability Density Function of the Inter-Arrival Times:* For daytime measurements, a generalization of the Poisson law (exponential PDF) proved to be a good approximation of the inter-arrival time frequency distribution, whereas in some cases with strongly varying telephone traffic (day and nighttime measurements), an average over the Poisson law according to Fano [20] yielded acceptable results. Fig. 4 shows both approximations. We concentrated on the daytime case with the higher calling rate.

The generalization of the exponential PDF $f(x) = \lambda e^{\lambda x}$ was carried out in the double logarithmic representation, leading to

$$\log_{10}\left[f_d(\xi)\right] = a_1 + a_4\xi - \frac{a_4}{\ln(a_2)} a_2^{(\xi - a_3)}, \quad \xi = \log_{10}(x) \tag{3}$$

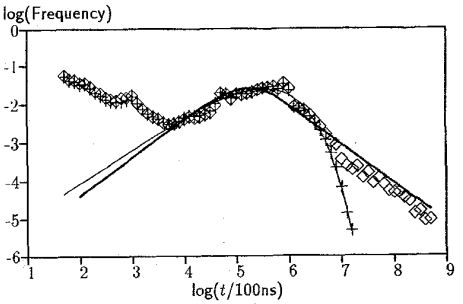


Fig. 4. Approximation of the density of the inter-arrival times (location: Kassel); ◇ Measurement days and nights; + Daytime measurement; — Generalized exponential density, (3); - Average over exponential densities, Fano [20].

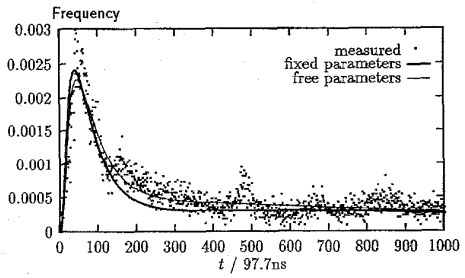


Fig. 5. Approximation of the impulse length density (location: Mayence).

which is equivalent to

$$f_d(x) = \frac{10^{a_1}}{\ln(10)}\, x^{a_4-1}\, 10^{-[a_4/\ln(a_2)]\, a_2^{[\log_{10}(x)-a_3]}} \qquad (4)$$

in linear representation. For the simulations described in Section V, we selected the coefficients of the location where also the impulses were taken from ($a_2 = 2.22$, $a_3 = 5.15$, $a_4 = 1.26$, $x = t/100$ ns). $a_1$ is a normalization constant and has to be chosen such that the integral over the density equals one.

*3) Probability Density Function of the Lengths:* The third frequency distribution that was investigated is the length distribution of the impulses. Although the frequency distribution looked quite different for every location, a sum of two log-normal densities was found to be an acceptable approximation. Fig. 5 shows a typical example. The log-normal approach is written as

$$f_l(t) = B \cdot \frac{1}{\sqrt{2\pi}s_1 t}\, e^{-(1/2s_1^2)\ln^2(t/t_1)} + (1-B)\cdot \frac{1}{\sqrt{2\pi}s_2 t}\, e^{-(1/2s_2^2)\ln^2(t/t_2)} \quad \text{for} \quad t > 0 \quad [f_l(t) = 0 \quad \text{for} \quad t \le 0]. \qquad (5)$$

As the parameters $s_1$, $s_2$, $t_1$, $t_2$ did not vary too much from location to location, they may be fixed to $s_1 = 7.68 \cdot 10^6$, $t_1 = 7.2$ $\mu$s, $s_2 = 10.24 \cdot 10^6$, $\mu_2 = 160$ $\mu$s.

For more detailed information, especially concerning the approximation parameters for all different locations, we refer the reader to [16].

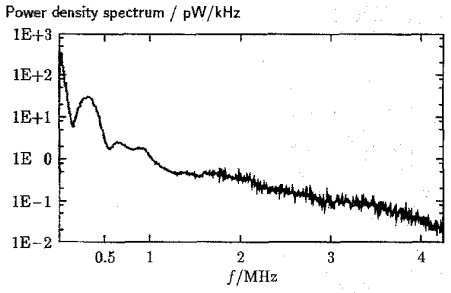


Fig. 6. Mean power density spectrum of all impulses measured at one location.

### C. Power Density Spectrum (PDS) and Phase Function

In many cases, the voltage and time statistics are not sufficient to model the impulse noise. The AKF or the PDS are necessary, too. The PDS of each stored impulse event was approximately calculated by an FFT.

The PDS of all impulses are not similar. Therefore, mean PDS of all impulses at different locations were determined. They also varied a lot. Nevertheless, the mean PDS of Fig. 6 is assumed to be a typical one. Spectral parts belonging to Gaussian background noise were eliminated. A very rough approximation of the mean PDS is the function

$$\frac{\overline{L(f)}}{\mathrm{dB}}\left(\frac{\mathrm{pW}}{\mathrm{kHz}}\right) = \begin{cases} -15\log_{10}\dfrac{f}{\mathrm{Hz}} + 80, & 5\,\mathrm{kHz} \le f \le 1.64\,\mathrm{MHz} \\ -29\log_{10}\dfrac{f}{\mathrm{Hz}} + 167, & 1.64\,\mathrm{MHz} \le f \le 4\,\mathrm{MHz} \end{cases} \qquad (6)$$

in double logarithmic representation. [The decrease per decade can be used for several measurements, but the frequency ranges and the constants in the back of (6) differ.] The variety of the impulse spectra is taken into account neither by the typical curve of Fig. 6 nor by the approximation in (6). A distribution of the PDS would accomplish this, but it would be far too complex.

For all applications where the real shape of impulses is important, their phase properties are necessary. An averaging over the phase of the FFT spectra of impulses would yield zero. But it showed out that phase differences between neighboring discrete spectral lines

$$\Delta\varphi(k\Delta f) = \varphi(k\Delta f) - \varphi[(k-1)\Delta f], \quad k \ge 1, \qquad (7)$$

which are comparable with the group delay, follow a typical function. An expression for $\Delta\varphi(k\Delta f)$ can be derived from a plot of maximum values in a histogram of measured phase differences for each discrete spectral line (Fig. 7). Values of measured phase differences around $\pi$ result from low spectral impulse energy in the corresponding frequency range. In the plot of Fig. 7, this behavior is evidently seen above the cut-off frequency of the anti-aliasing filter.

The measured phase difference can be approximated by

$$\Delta\varphi(k\Delta f) = \varphi_0 + \varphi_1\,(1 - e^{-k/\varphi_2}) - \varphi_3 k, \quad k \ge 1, \quad \Delta f = 5\,\mathrm{kHz}. \qquad (8)$$

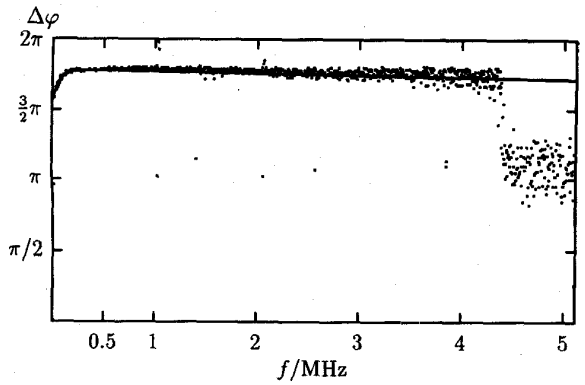


Fig. 7. Maximum values in a histogram of phase differences (dots) and their approximation (line).

At one location (Mayence), the set of parameters was: $\varphi_0 = 4.938$, $\varphi_1 = 0.672$, $\varphi_2 = 14.052$, $\varphi_3 = 2.1 \cdot 10^{-4}$. To be exact, the first two values ($k = 1, 2$) are substituted by the original data, because they are not too well described by the approximation. Now, using (7) and (8) and $\varphi(0) = 0$, the function of the typical impulse phase is determined. With this phase function and, e.g., the square root of the mean PDS of all impulses measured at one location, the spectrum of an impulse event, is derived. After applying the IFFT to this spectrum, we obtain an impulse, which can be seen as a "representative" impulse. It is plotted in Fig. 8 for one location. Obviously, it is similar to real measured impulses (cf., Fig. 2).

The representative impulse has been determined to show that the method of phase correction in the frequency domain results in realistic impulse shapes. For our simulations, it is senseless to use only a single representative impulse, because it cannot model the different existing impulse shapes.

### D. Simulation Options

Impulse noise can be simulated by using a data bank or a model based on densities (called generator model). As mentioned before, a representative impulse is not suitable. A Markov model as another alternative would be far too complex.

Until now, the CAP system was mostly simulated by a data bank access, because the complete generator model was not yet implemented from the beginning. For us and for all who might simulate impulse noise, the generator model may be preferable to the data bank access, because the original data have to be previously transferred to the data bank and the required storage must be very large (200 MBytes in compressed form). Nevertheless, just reading from a file should be faster than generating the impulses again for every simulation run.

*1) Data Bank Access:* We used the 51 200 stored impulse events of one location (Mayence). They are stored in compressed form on a magneto-optical disk or a hard disk. Their sample interval is 1/10.24 MHz = 0.0977 $\mu$s. During the simulation, the real measured data are read from the disk. The amplitudes of the impulses are not changed. The gap between two impulses is inserted as a sequence of zeros in such a way that the inter-arrival times of the simulated impulse noise are either constant (1.4 ms) or distributed according to the approximation in (4). Sequences for inter-arrival times less than 400 $\mu$s are not inserted, because they are already included within the impulse events. After the memory access, a sampling-rate adaptation has to be applied in order to adapt the sampling rate to the processing rate (chosen to be the 4-fold symbol rate) of the simulated configuration.

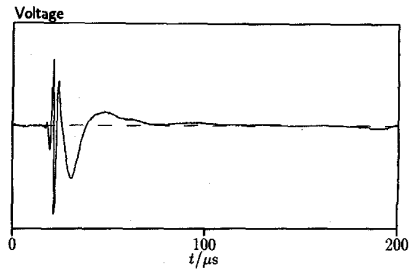


Fig. 8. Representative impulse derived from a mean PDS and the typical phase function (location: Mayence).

*2) Generator Model:* This method uses three specially developed random-number generators for the density functions of the voltages, the inter-arrival times, and the lengths of the impulses (see, [16]). Additionally, the impulse noise is filtered and, optionally, the impulse phase is corrected (Fig. 9).

The length generator (normal generator applying the transform method) produces length values. Then, a sequence of samples for an FFT block is constructed out of 200 preceding zeros (trigger delay), a specified number of generated voltage samples, and trailing zeros until the end of the block. The number of voltage samples equals the length. The block width has to be appropriately chosen. The voltage generator uses the rejection method.

In order to obtain an impulse event with the described spectral and phase properties, the following steps were implemented:

1) applying an FFT to this block,
2) multiplying the FFT spectrum by the square root of a typical mean PDS of all impulses measured at one location,
3) changing the phase of the multiplied spectrum according to the typical phase function of impulses, but keeping the absolute amplitude value (optional),
4) applying an inverse FFT,
5) optionally windowing at the output.

The block diagram in Fig. 9 offers several options and combinations thereof:

| | stochastic activation with windowing | stochastic activation without windowing | constant activation with windowing |
|---|---|---|---|
| without phase setting | | | |
| with phase setting | | | |

Examples of generated impulse events (without windowing at the output) are depicted in Figs. 10 and 11. In Fig. 10 (one impulse) the voltage samples were only filtered, i.e., the phase

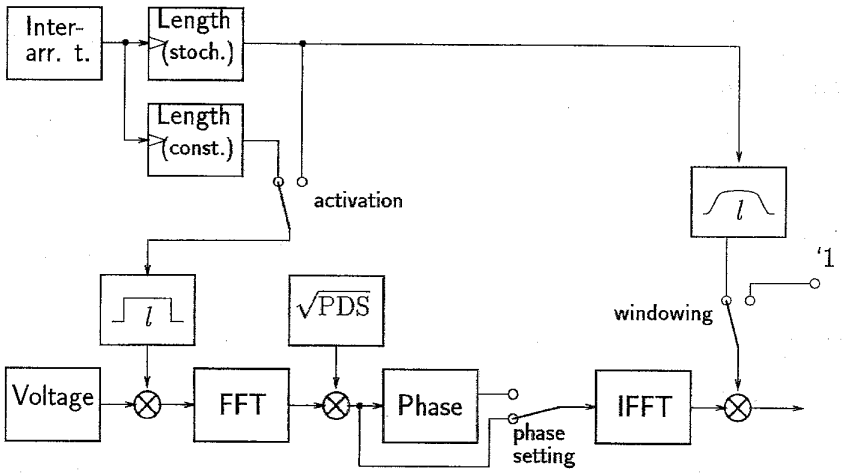


Fig. 9. Block diagram of the impulse-noise generator for simulations.

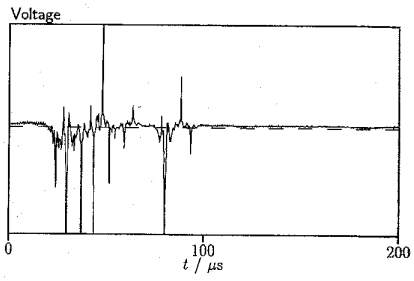


Fig. 10. Impulse event generated without phase correction.

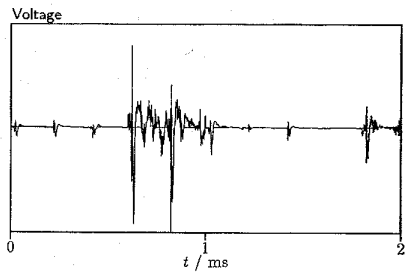


Fig. 11. Some impulse events generated with phase correction.

correction was not applied. The phase corrected impulses in Fig. 11 (10 impulses) are similar to the representative impulse of Fig. 8.

The inter-arrival time is generated using a modified strip method, which determines the gap filled with zeros between two impulse events. Inter-arrival times shorter than the length of the preceding event are not allowed.

If the described method is used, first, the densities of the voltage have to be modified, because the filter and phase operations change them. Analytic expressions for the densities at the input of the filter as a function of the densities at the output of the phase corrector, i.e., the desired densities according to (1) and (5) cannot be given.

For the voltage PDF $f_{in}(u)$ at the input, a feasible solution is the superposition of a Dirac onto the desired density $f_i(u)$,

$$f_{in}(u) = \epsilon f_i(u) + (1 - \epsilon)\,\delta(u) \tag{9}$$

with $\epsilon \in [0.01,\ 0.1]$.

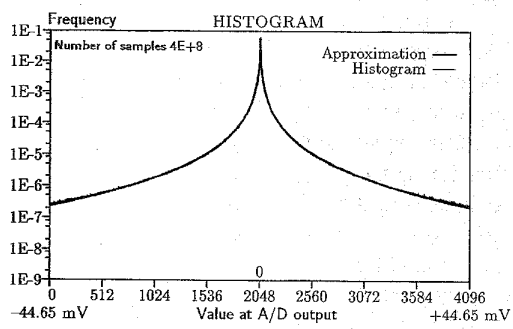


Fig. 12. Histogram of voltage samples generated without phase correction, without windowing, but with stochastic activation.

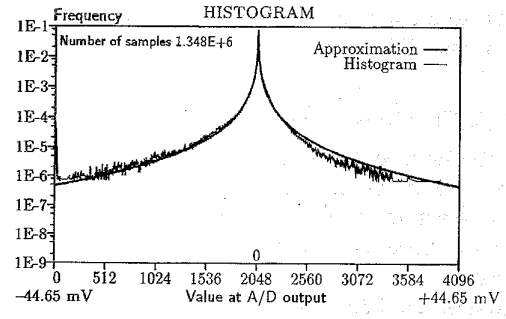


Fig. 13. Histogram of voltage samples generated with phase correction, with stochastic activation, but without windowing.

This means that the voltage generator inserts zeros. The Dirac approximately regenerates the desired density during the filter operation, providing the PDS *and* voltage density. The coefficients $u_0$ at the input and output of the filter are not the same. The coefficient at the input has to be determined beforehand by simulations. The insertion of a Dirac into the PDF is not generally applicable, but its usefulness depends on the shape of the PDF and the filter coefficients.

The histogram of filtered voltage samples without phase correction (with stochastic activation, without windowing) is plotted in Fig. 12. For comparison, Fig. 13 presents the corresponding histogram for filtered and phase corrected samples. Both follow the desired voltage density quite exactly. Only

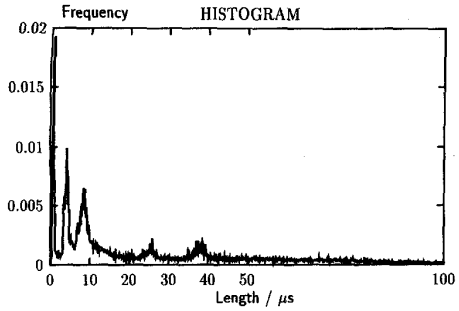


Fig. 14. Impulse length density with stochastic activation, but without windowing and without phase setting.

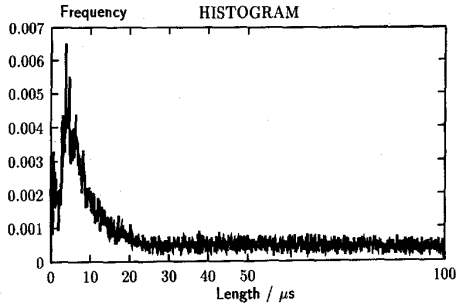


Fig. 15. Impulse length density with stochastic activation and with windowing, but without phase setting.

the phase corrected version becomes slightly unsymmetrical. This was expected, because also the representative impulse is not exactly symmetrical in its amplitudes. However, if a symmetrical frequency distribution is needed, this can be achieved by simply alternating the polarity of the impulse events after the phase correction.

More crucial are the length distribution and the length-energy relation, which is not discussed thoroughly in this paper.

Now, the influence of the phase setting will be outlined in some more detail.

The phase setting to prescribed values means that all impulse events are also more or less forced to a certain pulse shape similar to the representative impulse in Fig. 8. This is due to the fact, that unlike real impulses, no variation in the multiplied PDS is provided (we use the mean PDS), because this would complicate the model significantly. In reality, also the group delay function has a slight variation around the typical function. This can be modeled by adding a Gaussian random variable to the samples of the group delay function. This results in some variations of the impulse shape and looks a little more realistic. However, without a phase setting the generated impulses do not look like real impulses. Nevertheless, they have advantages in some of the statistical properties, like the length distribution and the length-energy relationship. A phase setting should only be applied, if the impulses should look like real impulses and the length distribution and the length-energy relation are of minor importance.

Without phase setting, a nearly linear length-energy relation is obtained. If additionally a length-dependent amplification is applied, even more complicated length-energy relations can be realized. This may change the voltage density, though. The length-distribution, however, is still the most critical aspect. Due to the shape of the impulse response that corresponds to $\sqrt{\text{PDS}}$, the length histogram has some discrete maxima at short lengths (see, e.g., Fig. 14). The shape is slightly improved by additional windowing (Fig. 15). For longer impulses, the length histogram looks similar to the desired distribution. Although the length distribution cannot be regenerated exactly, one should bear in mind that anyway, in reality, the length distribution showed the most variations dependent on the measurement location. Thus, the resulting length distribution is not unrealistic.

Some more details on the impulse generation will be published in [24].

## IV. Simulation Results Based on Real Measured Impulses and Constant Inter-Arrival Times (Worst-Case Study)

This section describes first results obtained when following the data bank approach. Transmission of a 64-CAP signal was studied under impulse noise which was taken from one location where the statistics were quite typical. The data set contains 51 200 impulse events and is completely used for the simulations. As a first step, described in this section, no inter-arrival time statistics are included. Instead, a constant inter-arrival time of 500 CAP symbols was chosen. This time span which equals 1.4 ms (2.048 Mb/s ADSL) is located just right of the minimum of the histogram of measured inter-arrival times in Fig. 4 and can be considered to be the starting point of the distribution, because further to the left, the frequency distribution is dominated by trigger intervals inside one impulse event. Thus, the results presented here resulted from a worst-case investigation. Two different loops were considered: a standard loop of 12 kft, 24 gauge and a quite long one of 4.25 km and 0.4 mm diameter. The totally uncoded error-burst length statistics are presented in Figs. 16 and 17, respectively. An error burst is defined to be separated by at least 10 error-free CAP symbols.

Of course, both figures show similarities to the original impulse length distribution in Fig. 5. The error length distribution has significant components at up to 30 CAP symbols for the short loop and about 80 symbols in the case of the long one. The corresponding symbol-error probabilities are $1.2 \cdot 10^{-3}$ and $3.3 \cdot 10^{-2}$, respectively. The uncoded error rate for the long loop is quite poor. Hence, no significant coding gains are expected from *any* error-correcting code. The following coding schemes were considered:

- 8-state trellis code (Wei),
- interleaved trellis coding (interleaving depth = 16),
- Reed–Solomon codes of length 135 symbols over GF($2^8$) with an error correcting capability of $t = 2, 3, 4$ together with interleaving of depths 18, 24, and 36,
- array codes as burst error correcting codes with $n_1$ rows and $n_2 = 2n_1 - 3$ columns and a maximum correctable single burst of length $n_1 - 1$.

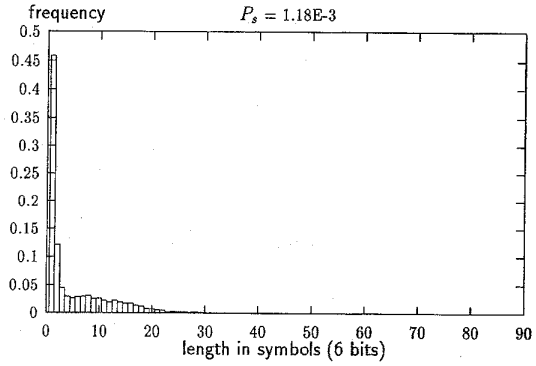


Fig. 16. Symbol-error length frequency distribution without coding (12 kft, 24 gauge).

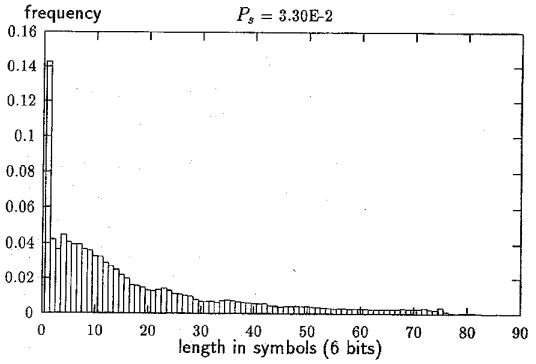


Fig. 17. Symbol-error length frequency distribution without coding (4.25 km, 0.4 mm).

The Reed–Solomon (RS) parameters are not optimized for the chosen impulse-noise environment, especially not for the fixed inter-arrival time. The parameters are the ones that were discussed in the corresponding standardization groups (ANSI). Nevertheless, at least the array size of the array code was chosen such that at most one impulse event occurs within an array. Ignoring the quite short inter-arrival time and regarding the length distribution in Fig. 16, the first set of RS parameters seems not to be too unrealistic. With $t = 2$ and an interleaving depth of $D = 18$, a burst-error correcting capability of $t \cdot D = 36$ is achieved which corresponds to $36 \cdot 8/6 = 48$ CAP symbols. This should be enough for the maximum burst lengths of the short loop.

We shall now consider the application of coded modulation. As an example, we applied an 8-state two-dimensional scheme. This improved the symbol error probability slightly in the case of the short loop ($8.36 \cdot 10^{-4}$), but was quite destructive with the long loop (0.56). Trellis coding together with Viterbi decoding can of course not handle severe bursty noise. The error-length distribution in Fig. 18 (short loop) shows similarities to the uncoded case except that short error events are reduced. Even an interleaved trellis coding with an interleaving depth of up to 16 is not very effective. The symbol error probability is further slightly reduced to $5.71 \cdot 10^{-4}$ (short loop). The error-length distribution is shown in Fig. 19. The relatively strong single error component is due to the underlying burst definition: a new error burst starts after

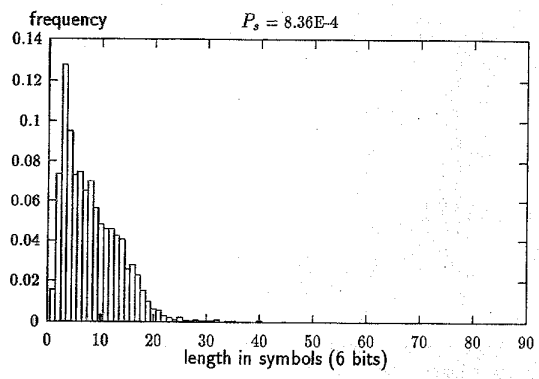


Fig. 18. Symbol-error length frequency distribution with included 2-dimensional trellis coding (12 kft, 24 gauge).

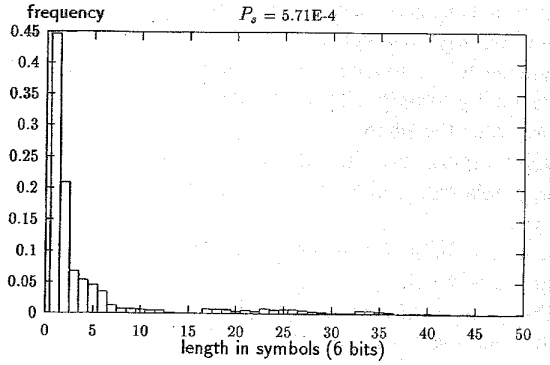


Fig. 19. Symbol-error length frequency distribution with included interleaved trellis coding (interleaving depth: 16; 12 kft, 24 gauge).

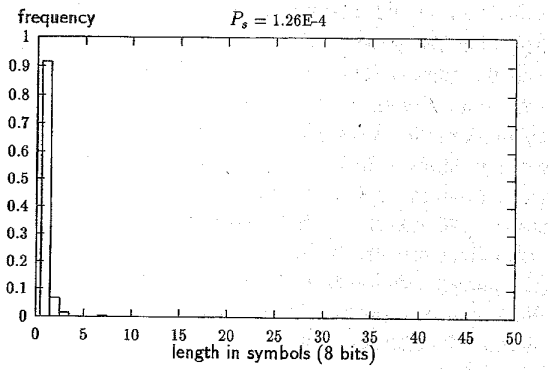


Fig. 20. Symbol-error length frequency distribution with included Reed–Solomon code ($t = 2$, $D = 18$; 12 kft, 24 gauge).

at least 10 error-free symbols. In the sequel, only results for the short loop are given, unless otherwise stated.

A very effective burst correction is expected and obtained with RS codes. Without any additional trellis coding and with an interleaving depth of 18 symbols (8 bits), we achieved symbol (8 bits) error rates of $1.26 \cdot 10^{-4}$, $2.06 \cdot 10^{-5}$, and $2.10 \cdot 10^{-6}$ (bit-error prob. = $8.17 \cdot 10^{-7}$) for $t = 2$, 3, and 4, respectively. The length statistic for $t = 2$ is given in Fig. 20. The statistics for $t = 3$ and $t = 4$ look very similar. With additional trellis coding, the error probabilities are further reduced to $5.84 \cdot 10^{-5}$ ($t = 2$), $4.91 \cdot 10^{-6}$ ($t = 3$) and actually no error for $t = 4$.

With the long loop and $t = 2$, the symbol-error probability was about $3.9 \cdot 10^{-2}$ for interleaving depths between 18 and 36. Hence, effectively no coding gain is obtained with the long loop. Even for the short loop, an increase of the interleaving depth does not improve the error probability much. For $t = 2$ and no additional trellis coding, the symbol error rates are $1.26 \cdot 10^{-4}$, $9.63 \cdot 10^{-5}$, and $7.46 \cdot 10^{-5}$ for $D = 18$, $D = 24$, and $D = 36$, respectively. As already mentioned, the interleaving depth of $D = 18$ together with $t = 2$ is reasonable as far as the uncoded symbol-error length distribution is concerned. On the other hand, a further increase in the interleaving depth means that more impulse events fall into one interleaver matrix, thereby possibly exceeding the error-correcting capability of the RS code.

As an alternative to RS codes, array codes with a diagonal readout were investigated. Their advantage is their relatively low decoding complexity due to the fact that the component codes are simple parity-check codes. Their disadvantage is that they are pure (single) burst correcting which means that additional random errors can easily lead to an uncorrectable error pattern. Furthermore, the probability of wrong correction is not as small as for RS codes. However, if impulse noise is dominant, array codes may be a worthwhile alternative.

Array codes are described by three parameters: $n_1$, the number of rows, $n_2$, the number of columns, and $s$, the shift between the output diagonals. We only considered $s = 1$. One can show (see, [21], [22], and [7]) that such array codes with $n_2 \geq 2n_1 - 3$ are capable of correcting cyclic bursts of at most $n_1 - 1$ bits or symbols. The term "symbol" stands for the components of nonbinary array codes, where each array component consists of a vector of binary digits (or of other group elements). The array code is made up from parity checks in rows and columns. In the case of binary component vectors, the parity checks are computed separately for every component. An exemplary array with the readout cycle and the location of the parity checks is shown subsequently.

| | | | | | | | | |
|---|---|---|---|---|---|---|---|---|
| 0 | 6 | 12 | 18 | 24 | 30 | 36 | 42 | 48 |
| 49 | 1 | 7 | 13 | 19 | 25 | 31 | 37 | 43 |
| 44 | 50 | 2 | 8 | 14 | 20 | 26 | 32 | 38 |
| 39 | 45 | 51 | 3 | 9 | 15 | 21 | 27 | 33 |
| 34 | 40 | 46 | 52 | 4 | 10 | 16 | 22 | 28 |
| 29 | 35 | 41 | 47 | 53 | 5 | 11 | 17 | 23 |

(10)

The performance of array codes can be further improved by reducing the coding/decoding delay. A proposal to decrease the coder-delay has been made in [7], leading to an overall reduction by about 35%. The scheme uses three different filling modes together with a prefilled area of the array. The filling cycle for (10) is given as follows:

| | | | | | | | | |
|---|---|---|---|---|---|---|---|---|
| 0 | 5 | 9 | 17 | 19 | * | * | 12 | @ |
| 24 | 1 | 6 | 10 | 18 | * | * | 13 | @ |
| 25 | 29 | 2 | 7 | 11 | * | * | 14 | @ |
| 26 | 27 | 28 | 3 | 8 | * | * | 15 | @ |
| 20 | 21 | 22 | 23 | 4 | * | * | 16 | @ |
| @ | @ | @ | @ | @ | @ | @ | @ | — |

(11)

$*$: prefilled positions, @: parity symbols, $-$: parity-of-parities (left empty).

TABLE I
OVERVIEW OVER THE SIMULATION RESULTS WITH *CONSTANT* INTER-ARRIVAL TIMES

| | without trellis code | with trellis code | with interleaved trellis code |
|---|---|---|---|
| short loop | | | |
| no outer code | $1.18 \cdot 10^{-3}$ | $8.36 \cdot 10^{-4}$ | $5.71 \cdot 10^{-4}$ |
| RS, $t = 2$, $D = 18$ | $1.26 \cdot 10^{-4}$ | $5.84 \cdot 10^{-5}$ | $7.57 \cdot 10^{-5}$ |
| RS, $t = 3$, $D = 18$ | $2.06 \cdot 10^{-5}$ | $4.91 \cdot 10^{-6}$ | |
| RS, $t = 4$, $D = 18$ | $2.10 \cdot 10^{-6}$ | no error | $1.40 \cdot 10^{-6}$ |
| RS, $t = 2$, $D = 24$ | $9.63 \cdot 10^{-5}$ | | |
| RS, $t = 2$, $D = 36$ | $7.46 \cdot 10^{-5}$ | | |
| ARRAY, $n_1 = 13$ | | $8.85 \cdot 10^{-5}$ | |
| ARRAY, $n_1 = 100$ | | $1.01 \cdot 10^{-3}$ | |
| long loop | | | |
| no outer code | $3.30 \cdot 10^{-2}$ | $5.6 \cdot 10^{-1}$ | $4.5 \cdot 10^{-2}$ |
| RS, $t = 2$, $D = 18$ | $3.85 \cdot 10^{-2}$ | | |
| RS, $t = 2$, $D = 36$ | $3.88 \cdot 10^{-2}$ | | |

The decoding algorithm was taken from [21], [22], and consists in principle of a search for the largest consecutive cyclic range of columns whose parity checks are not violated. The burst starts right after this range. The exact burst location in a cyclically continued diagonal is determined by jointly considering the parity violations in the rows, too. Thus, column and row parity violations represent the actual error pattern.

Two exemplary simulation runs were carried out. In one case, the array size was adapted to the inter-arrival time with $n_1 = 13$ and $n_2 = 2n_1 - 3 = 23$, whereas the parameters in the second run were $n_1 = 100$ and $n_2 = 2n_1 - 3 = 197$. The symbols were chosen from GF($2^8$) as for the RS codes. Together with included trellis coding, symbol error rates of $8.85 \cdot 10^{-5}$ and $1.01 \cdot 10^{-3}$, respectively, were achieved. The second result reveals the drawback of single-burst correcting error codes when multiple bursts occur within one array. Nevertheless, the first result is comparable to an RS code with $t = 2$ and $D = 18$, but with lower rate [$1 - (13 + 23 - 1/13 \cdot 23) = 0.883$]. With real inter-arrival times, the array size may be further increased, thereby increasing the rate, too.

An overview over all simulation results is given in Table I.

## V. SIMULATION RESULTS WITH STOCHASTIC INTER-ARRIVAL TIMES

When stochastic inter-arrival times according to Section III-B-2 are used, more realistic results for the error probabilities are obtained. Hereto, the specially developed generator for the inter-arrival times was used with the set of coefficients also mentioned in Section III-B-2. Table II shows the simulation results.

First, by using realistic inter-arrival times, the totally uncoded symbol (6 bits)-error probability is reduced significantly to $2.8 \cdot 10^{-5}$ for the short loop and $7.82 \cdot 10^{-4}$ for the long loop. An RS code with $t = 2$ reduces these to $1.14 \cdot 10^{-7}$ and $2.98 \cdot 10^{-4}$ (8-bit symbols), respectively. We conclude that such a simple RS code yields acceptable results for the short loop, whereas the protection for the long loop is not sufficient. A $t = 4$ code further decreased the symbol-error probability to $3.93 \cdot 10^{-5}$ in the case of the long loop. An increase in the interleaving depth then leads to a reasonable error performance of $4.92 \cdot 10^{-6}$, because with real inter-arrival times, an increase of the interleaving depth is not as

TABLE II
OVERVIEW OVER THE SIMULATION RESULTS WITH *STOCHASTIC* INTER-ARRIVAL TIMES

| | without trellis code | with trellis code |
|---|---|---|
| short loop | | |
| no outer code | $2.80 \cdot 10^{-5}$ | $1.6 \cdot 10^{-5}$ |
| RS, $t = 2$, $D = 18$ | $1.14 \cdot 10^{-7}$ | $5.73 \cdot 10^{-9}$ |
| RS, $t = 3$, $D = 18$ | 0 | 0 |
| RS, $t = 4$, $D = 18$ | 0 | 0 |
| RS, $t = 2$, $D = 24$ | $4.97 \cdot 10^{-8}$ | $6.65 \cdot 10^{-8}$ |
| RS, $t = 2$, $D = 36$ | $3.72 \cdot 10^{-9}$ | 0 |
| ARRAY, $n_1 = 13$ | $3.86 \cdot 10^{-6}$ | $2.71 \cdot 10^{-6}$ |
| ARRAY, $n_1 = 23$ | $4.50 \cdot 10^{-6}$ | $2.07 \cdot 10^{-6}$ |
| ARRAY, $n_1 = 33$ | $5.53 \cdot 10^{-6}$ | $2.16 \cdot 10^{-6}$ |
| long loop | | |
| no outer code | $7.82 \cdot 10^{-4}$ | |
| RS, $t = 2$, $D = 18$ | $2.98 \cdot 10^{-4}$ | |
| RS, $t = 4$, $D = 18$ | $3.93 \cdot 10^{-5}$ | |
| RS, $t = 4$, $D = 36$ | $4.92 \cdot 10^{-6}$ | |

critical as in the case of the previous section where a rather short inter-arrival time resulted in multiple bursts within the interleaver matrix.

These results show that even with quite weak RS codes, an acceptable error protection in an impulse-noise environment can be guaranteed. Array codes achieve a symbol-error probability of $3.86 \cdot 10^{-6}$ for the short loop with $n_1 = 13$. A further increase of the array size is disadvantageous due to the restriction of the error-correcting capability to only one burst.

In order to prove the usefulness of our complete generator model, a few simulation runs have been performed with impulses derived from the generator, too. The results looked quite similar for cases with stochastic activation and windowing, but without phase correction. Since the phase correction changes the length distribution significantly, this has a great influence on code performance.

## VI. SUMMARY

All the investigations were based on the data of an impulse-noise measurement campaign, carried out by German Telekom. This survey and its results, the statistical modeling of impulse noise, were shortly described.

Results for the generation of impulse noise by dedicated noise generators following the desired statistics and first results for the error performance of ADSL-CAP (asymmetrical digital subscriber line—carrierless amplitude/phase modulation) transmission under impulse-noise disturbance were presented.

It was shown that nearly all important statistical properties can be fulfilled by applying a combined generator structure consisting of a voltage generator and generators for the impulse lengths and inter-arrival times together with a filtering and, optionally, a phase correction operation. Especially, it was achieved that the filtering and phase correction do not change the voltage density. The phase correction is essential, if realistic impulse shapes are desired. However, it has a certain effect on the length distribution and its use should therefore be restricted to cases where the impulse shape is of more interest than the length distribution.

For the simulation results presented herein, mostly only one component of the generator model was used, the inter-arrival time generator. This was reasoned by the fact that the complete generator configuration was not yet available when the simulations were carried out. Therefore, a data bank approach was pursued, selecting stored impulse events from one location of the whole measurement campaign. First, a constant, quite short inter-arrival time was chosen to obtain some worst case results. In a second phase, real inter-arrival times were generated by the specially developed generator. The following coding schemes were studied: 8-state trellis code, interleaved trellis coding, Reed–Solomon codes with symbol interleaver, and array codes with diagonal readout. It was found that relatively weak RS codes with a correcting capability between 2 and 4 symbols together with an interleaving depth of 18 (or slightly more) yielded an acceptable error performance on two exemplary loops (12 kft, 24 gauge and 4.25 km, 0.4 mm). Trellis-coding may be abandoned. It gains not much for the first loop (except the nevertheless interesting case with stochastic inter-arrival times and an RS code with $t = 2$ and interleaving depth of 18), but is disastrous for the second one. Array codes may be an alternative in an impulse noise dominated environment and have the advantage of very low decoding complexity.

## REFERENCES


[1] K. Sistanizadeh, "Ad hoc meeting report on ADSL loop reach, channel rates, & PSD," *T1E1.4 Ad Hoc Meeting Contribution T1E1.4/93-150,* May 11, 1993.

[2] M. Sorbara and R. A. Schreibmaier, "Carrierless AM/PM (CAP) asymmetrical digital subscriber line (ADSL) transceiver," *CAP ADSL Transceiver System Requirements,* AT&T, Sept. 1993.

[3] M. Sorbara, J.-J. Werner, and N. Zervos, "Carrierless AM/PM," *HDSL Contribution to T1E1.4,* T1E1.4/90-154, Sept. 1990.

[4] J.-J. Werner, "Impulse noise in the loop plant," in *Proc. ICC.*, 1990.

[5] G. Ungerboeck, "Channel coding with multi-level/phase signals," *IEEE Trans. Inform. Theory,* vol. IT-28, no. 1, pp. 55–67, Jan. 1982.

[6] Lin and Costello, *Error Control Coding: Fundamentals and Applications.* Englewood Cliffs, NJ: Prentice-Hall, 1983.

[7] W. Henkel and H. Y. Chung, "A new filling procedure to reduce the delay of burst-error correcting array codes," *Electron. Lett.,* vol. 30, no. 6, pp. 465–466, Mar. 17, 1994.

[8] CCITT Study Group XVII, "Recommendation V.32 for a family of 2-wire duplex modems operating at data signaling rate of up to 9600 bps for use on the general switched telephone network and on leased telephone-type circuits," Document AP VIII-43-E, May 1984.

[9] J. Nadenau, "Typische Störspannungen in Fernsprechvermittlungsstellen," *NTZ,* vol. 15, pp. 236–240, 1962, (in German).

[10] J. M. Berger and B. Mandelbrot, "A new model for error clustering in telephone circuits," *IBM J. Res. Dev.,* vol. 7, pp. 224–236, 1963.

[11] J. H. Fennick, "Amplitude distributions of telephone channel noise and a model for impulse noise," *Bell Syst. Tech. J.,* vol. 48, pp. 3243–3263, 1969.

[12] H.-W. Wellhausen and J. Fahrendholz, "Digitalsignalübertragung auf symmetrischen Ortsverbindungs- und Ortsanschlußkabeln," *Technical Report 442 TB 71,* Darmstadt, 1986.

[13] W. F. Müller and H. Lubenow, "Störimpulse in Nachrichtenkanälen," *Nachrichtentechnik, Elektronik,* vol. 38, pp. 8–9, 1988.

[14] K. Széchényi and K. Böhm, "Impulsive noise limited transmission performance of ISDN subscriber loops," in *Proc. ISSLS,* 1988, pp. 2.3.1–2.3.6.

[15] K. Széchényi, "On the NEXT and impulse noise properties of subscriber loops," in *Conf. Record GLOBECOM,* 1989, pp. 1569–1573.

[16] W. Henkel and T. Kessler, "A wideband impulsive noise survey in the German telephone network: statistical description and modeling," *AEÜ,* vol. 48, no. 6, pp. 277–288, Nov./Dec. 1994.

[17] ——, "Statistical description and modeling of impulsive noise on the German telephone network," *Electron. Lett.,* vol. 30, no. 12, pp. 935–936, June 9, 1994.

[18] J. W. Cook, "Wideband impulsive noise survey of the access network," *BT Tech. J.,* vol. 11, pp. 155–162, 1993.

[19] C. F. Valenti and K. Kerpez, "Analysis of wideband noise measurements and implications for signal processing in ADSL systems," presented at ICC '94, Houston, TX, 1994.

[20] R. M. Fano, "A theory of impulse noise in telephone networks," *IEEE Trans. Commun.*, vol. COM-25, pp. 577–588, 1977.
[21] H. C. A. van Tilborg, "An overview of recent results in the theory of burst-correcting codes," *Springer Lecture Notes in Computer Science 388*, pp. 164–184, 1988.
[22] M. Blaum, P. G. Farrell, and H. C. A. van Tilborg, "A class of burst error-correcting array codes," *IEEE Trans. Inform. Theory*, vol. IT-32, no. 6, pp. 836–839, Nov. 1986.
[23] T. Kessler, W. Henkel, and H. Y. Chung, "A wide-band impulse-noise survey in the German telephone network—Statistical description," submitted to *CTMC '95*.
[24] W. Henkel, T. Kessler, and H. Y. Chung, "A wide-band impulse-noise survey in the German telephone network—Modeling and simulation," submitted to *CTMC '95*.
[25] W. Henkel and H. Y. Chung, "Coded 64-CAP ADSL in an impulse-noise environment—Simulation results," submitted to *Globecom '95*.

**Werner Henkel** (S'87–M'89) was born in Gelnhausen, Germany, on April 27, 1960. He studied electrical engineering (telecommunications) at TH Darmstadt, where he received his diploma degree in 1984. From 1984 to 1989, he had a contract as a research assistant at TH Darmstadt and received his Ph.D. degree in 1989. His thesis was on coding with complex numbers. During this time, he also held lectures at FH Frankfurt.

In 1989, he joined the Research Center of Deutsche Telekom. His work concentrates on digital communications, especially coding, coded modulation, synchronization, equalizing, neural networks, and channel modeling. He also held internal courses on information theory and coding. From September 1993 until March 1994, he was on a sabbatical leave at AT&T Bell Laboratories, Middletown, NJ, where he worked on high-rate subscriber line transmission in an impulse-noise environment and burst-error correcting codes. He has contributed publications on analog, codes, coding and interpolation, Toeplitz algorithms, coded modulation, synchronization, channel modeling, burst error correcting codes, and A/D-conversion.

**Thomas Kessler** was born in Kassel, Germany, on February 22, 1961. He received his diploma degree in communications engineering from the Technical University of Brunswick, Germany, in 1987.

Since then, he has been with the Research Center of Deutsche Telekom, department of digital transmission systems. He was engaged in the error-performance analysis of quaternary transmission systems, the digital signal processing for equalizers, and the design of rotationally invariant trellis codes. He was also involved in the hardware implementation of Viterbi decoders for both satellite and cable applications. His current interest is in the analysis of measured impulse noise on telephone cables and its modeling for computer simulations of ADSL systems.

**Hong Y. Chung** (S'83–M'85) is a member of Technical Staff at AT&T Bell Laboratories where he has been working in the areas of digital communications research and development for various industrial applications since 1985. His areas of research interests include coded modulation, digital signal processing, and power- and bandwidth-efficient digital transmissions.